



Comparative experimental and mathematical analysis on removal of dye using raw rice husk, rice husk charcoal and activated rice husk charcoal: batch, fixed-bed column, and mathematical modeling

Niladri Saha¹ · Lopamudra Das¹ · Papita Das¹ · Avijit Bhowal¹ · Chiranjib Bhattacharjee¹

Received: 2 July 2021 / Revised: 22 September 2021 / Accepted: 24 September 2021 / Published online: 21 October 2021
© The Author(s), under exclusive licence to Springer-Verlag GmbH Germany, part of Springer Nature 2021

Abstract

A methodology involving rice husk (RH), rice husk charcoal (RHC), and activated rice husk charcoal (ARHC) as an effective adsorbent to eliminate malachite green dye from aqueous solution using adsorption process by varying the pH, initial dye concentration (mg/L), contact time, temperature, and adsorbent doses (g/L). The surface characteristics were observed under scanning electron microscopy (SEM), and Fourier transform infrared (FTIR) spectroscopy was used to identify the chemical bonds present on the adsorbent surface. Data obtained from adsorption system at equilibrium condition were fitted to isotherm models such as Langmuir and Freundlich model where it was found that unlike raw RH and RHC equilibrium, data for ARHC fitted best to Langmuir model with 1000 mg/g as maximum adsorption capacity at 303 K, indicating homogeneous monolayer adsorption by the mesopores. The adsorption kinetics for all three adsorbents were observed to fit the pseudosecond-order model better. The negative value of ΔH and ΔS obtained from the thermodynamic study indicates that the process is exothermic and involves an associative mechanism respectively. Boyd plot was used to understand the mass transfer mechanism. Moreover, fixed-bed column studies were performed using ARHC as the adsorbent. At different experimental conditions such as inlet flow rate (Q), initial dye concentration (C_0), bed height (L_b), and pH, it was observed that the adsorption capacity (k_d^*) of MG dye on ARHC in a fixed bed continuous flow in a column mode, ranged between 0.008 and 0.177 (g/g). Present investigation and comparison with other reported adsorbents concluded that RH, RHC, and ARHC can be used as efficient and environment-friendly adsorbents for the removal of dissolved malachite green from contaminated water. However, ARHC was proved to be the best-suited candidate among the three adsorbents.

Keywords Isotherm · Kinetics · Thermodynamics · Mass transfer · Fixed bed column · Mathematical modeling

1 Introduction

Industrial wastewater contains a wide variety of pollutants that can cause severe damage to the environment if discharged into ponds, lakes, rivers, or seas without any treatment. They not only pollute the water body or the aquatic environment but also deplete the groundwater table causing contamination in drinking water. Among such chemicals, dye is used in several sectors like textile, cosmetic, plastic, paper, leather, and pigment industries.

Synthetic dyes like alizarin, amaranth, Congo red, gentian violet, malachite green, methyl red, methylene blue, Sudan,

tartrazine, and Tropaeolin are found to be harmful not only for aquatic species but also extremely toxic for humans. The toxicity of the dyes and their subsidiary chemicals extends from tropical irritation to carcinogenicity and mutagenicity, depending on the exposure [1].

Malachite green (MG) is used as a primary contaminant in this study. It is a commonly used dye for textile, paper, and fishery. It is a triphenylmethane dye. *Oomycete Saprolegnia* and *Ichthyophthirius multifiliis* are algae that infect fish eggs. MG is actively used to treat such algal contaminations in commercial aquaculture. Malachite Green also has effective antibacterial properties and is a popular treatment in freshwater aquaria. Application of malachite green in the aquaculture industry is illegal though it is an inexpensive and effective antibacterial, topical fungicide, and parasiticide. The reason being, malachite green is readily absorbed by fish and metabolically reduced to lipophilic

✉ Niladri Saha
niladrianjan@gmail.com

¹ Jadavpur University, Kolkata, India

leucomalachite green (LMG). The reduced form of malachite green has a long residence time in fish tissues and is eventually introduced to the food chain causing bio magnifications. Moreover, this dye is also carcinogenic and may lead to organ damage on long-term exposure [2].

Treatments of industrial wastewater use various methods like filtration, precipitation, catalytic degradation, electrolytic separation, and many others [3]. Among such methods, adsorption is one of the most efficient and cost-effective methods owing to its cost-effectiveness and good capacity to remove the contaminant from industrial effluent [4].

The adsorption process is a less energy-intensive unit operation compared to others. It is an advantage process due to sludge-free operation and complete removal of contaminants. These factors make it one of the attractive options for the treatment of effluent in the industries. The adsorbents used to remove contaminants like metal ions and phenolic compounds; organic matter and harmful dyestuff may vary from materials like activated carbon, silica gel, zeolite, and alumina to renewable materials like biological and agricultural wastes in different forms [5].

Unconventional approaches based on the use of natural, inexpensive biological, or agricultural materials for effluent treatment have been of great interest to researchers across the world in the recent past. Utilization of plant-derived materials like sunflower seed hull, banana pith, vine, eucalyptus bark, hazelnut shell, neem leaves, luffa cylindrical fiber, soybean hull, neem sawdust, agricultural waste byproducts, and teak wood bark were used as adsorbents for the purification of wastewater [6]. Biochar derived from various agricultural wastes such as sugarcane bagasse [7], peanut shell [8], rubber wood sawdust [9], Periwinkle shell [10], Ceibapentandra hulls [11], and coir pith [12] has been reported to be a suitable candidate for effluent adsorption.

India is one of the leading producers of rice in the world, therefore generating a considerable amount of rice husk. According to recent USDA data, India produces approximately 120 million tons of rice from 44.5 million hectares. This leads to rich husk extraction of about 24 million per year. The majority of the husk is consumed by the rice mills to generate heat for the boilers leading to an enormous amount of rice husk ash or rice husk charcoal [13]. Disposal of RHA is a matter of concern for the mills as unplanned dumping of RHA leads to leaching of various chemicals like silicon dioxide, iron, calcium oxide, sulfur trioxide, magnesium oxide, manganese oxide, and many others to the groundwater table [14].

On the other hand, studies were conducted to see the efficacy of rice husk as a usable adsorbent [15, 16]. Hence this study is focused on the adsorption technique using both raw rice husk and rice husk charcoal for decolorization of malachite green dye contaminated effluent.

Raw RH facilitates dye adsorption through cumulative adsorption capabilities of cellulose, hemicellulose, lignin, and others. This adsorption capabilities of raw RH can be enhanced by the removal of all volatile matter through carbonization; leaving only fixed carbon matter behind.

The prime objective of this study was to assess the suitability of raw rice husk (RH), charcoal obtained from rice husk (RHC), and activated rice husk charcoal (ARHC) for the removal of malachite green dye. Rice husk was chosen as the primary source of adsorbent because of its granular structure, local availability at very low cost, chemical stability, biocompatibility, and biodegradability.

Moreover this study also aims at solution of waste management issues in rice production industry that can be sustainably recycled to generate highly efficient adsorbents to treat waste water which was considered as one of the primary novelties of this study.

2 Materials and methods

2.1 Materials used

The malachite green dye of 99.99% purity used as a contaminant in this study was supplied by Loba Chemie. Sodium hydroxide (NaOH) was used to remove silica from RHC in the form of sodium silicate. Sodium hydroxide and hydrochloric acid (HCl) were also used to adjust the pH of the adsorption system. Both sodium hydroxide of 99.99% purity and hydrochloric acid of 37% concentration were supplied by Merck.

2.2 Collection and treatment of raw rice husk (RH)

Rice husk used in this study was collected from farmers of the Medinipore district. In this study, raw rice husk of Swarna (IET 5656) variety was used. It was washed several times with distilled water and was filtered using a strainer. It was then oven-dried at 393 K or 120 °C and cooled. The washed rice husk was ground and sieved with 60 mesh size strainer, i.e., particle size $\leq 250 \mu\text{m}$. The finely ground powder was stored in a cool dry place in an airtight bottle.

2.3 Preparation of rice husk charcoal (RHC)

Finely ground raw RH was charred at 673 K or 400 °C for 1 h in a ceramic crucible with N_2 purging to avoid ash formation. The carbonization temperature of 673 K was finalized to avoid waste of energy as no remarkable weight loss was observed at temperature higher than 673 K. When cooled the obtained charcoal was ground and sieved using 60 and 100 mesh size strainer, i.e., particle size lesser than 250 and 150 μm , respectively. Prepared adsorbents were stored in an airtight bottle.

2.4 Activation of rice husk charcoal

The creation of micropores by removal of the silica is the main principle behind the activation of rice husk charcoal. To activate the carbonized RH, RHC was optimized to be treated for 2 h with 4%w/w NaOH and heated to 393 K or 120°C accompanied by vigorous stirring. The residue obtained is activated RHC (ARHC) and the filtrate obtained is sodium silicate, a byproduct that is a precursor in the production of precipitated silica [17].

2.5 Preparation of dye solution

Malachite green (MG) is a cationic dye. Various concentrations of MG dye were used as wastewater for this study. Different concentrations of dye were prepared from a stock solution of 100 mg/L by dilution with distilled water. UV–Vis Spectrophotometer (Perkin Elmer Lambda 365) was used to determine the absorbance of the dye at 617 nm wavelength (λ_{max}). The standard calibration curve was plotted by fitting to Beer-Lambert’s law.

2.6 Batch adsorption experiments

Equilibrium adsorption of the solute using raw rice husk (RH), rice husk charcoal (RHC), and activated rice husk charcoal (ARHC) were carried out in a set of 100 mL Erlenmeyer flasks at an agitation speed of 120 rpm, at varying temperature ranges (25 to 45° C), adsorbent dose (2 to 10 g/L) based on the dry weight of adsorbent, initial dye concentrations of (5 to 20 mg/l), and fixed pH of 7. Samples were collected at 15-min intervals until equilibrium was established. Collected samples were centrifuged at 10,000 rpm for 10 min. The supernatant was analyzed by UV–Vis Spectrophotometer for dye contents at 617 nm. Each experiment was conducted thrice and was expressed as the mean value of the obtained results. MG removal at any given time(t) and equilibrium conditions, respectively [7, 18, 19]:

$$q_t = (C_0 - C_t) \times \frac{V}{W} \tag{1}$$

$$q_e = (C_0 - C_e) \times \frac{V}{W} \tag{2}$$

where V (L) denotes experimental solution volume and W (g) stands for the weight of the adsorbent used. C_0 and C_t (mg/L) denote the initial dye concentration and the concentration of remaining dye at a given time, respectively. C_e stands for equilibrium concentration, where q_t (mg g⁻¹) and q_e (mg/g) were denoted as MG removal on both RH and ARHC.

The dye adsorption efficiency was determined by the following formula in terms of dye removal percentage [5].

$$\%Removal = (C_0 - C_t) \times \frac{100}{C_0} \tag{3}$$

2.7 Adsorption isotherm

The batch adsorption data was modeled using Langmuir and Freundlich to identify adsorption behavior. The Langmuir isotherm model is expressed as [19]

$$\frac{C_e}{q_e} = \frac{1}{k_L q_m} + \frac{C_e}{q_m} \tag{4}$$

where C_e is the concentration of adsorbate measured at the time of equilibrium condition and q_e is adsorption capacity (mg/g). k_L is the Langmuir rate constant, and q_m stands for maximum monolayer adsorption capacity (mg/g).

Freundlich isotherm is another popular model that is expressed as [19]:

$$\log q_e = \log k_f + \frac{1}{n} \log C_e \tag{5}$$

where k_f is the Freundlich isotherm rate constant and n is the empirical constant.

2.8 Adsorption kinetics

Pseudofirst-order and second-order kinetic models were fitted with the obtained adsorption data.

Following are the representation of both the kinetic model Pseudo 1st order [7]

$$\log(q_e - q_t) = \log q_e - \frac{k_1 t}{2.303} \tag{6}$$

where k_1 is the first-order rate constant. Pseudo 2nd order can be expressed in linear form

$$\frac{t}{q_t} = \frac{1}{k_2 q_e^2} + \frac{t}{q_e} \tag{7}$$

Here, k_2 is the second-order rate constant with the unit g/mg min.

2.9 Thermodynamic experiments

All the thermodynamic parameters and the characteristics of the adsorption system were derived by the following empirical formula [20]:

$$K_c = \frac{C_a}{C_e} \tag{8}$$

$$\Delta G = -RT \ln K_c \quad (9)$$

$$\ln K_c = -\frac{\Delta G}{RT} = -\frac{\Delta H}{RT} + \frac{\Delta S}{R} \quad (10)$$

where K_c is the distribution coefficient of adsorption, G is Gibb's free energy difference, and S is the entropy variations. Similarly, H , R , and T symbolize enthalpy variation, ideal gas constant, and absolute temperature, respectively. Here C_a denotes the amount of dye adsorbed per unit mass of adsorbent.

2.10 Mechanism and mass transfer experiments for batch adsorption

The resulted data from the batch study was fitted to the intraparticle diffusion model proposed by Webber and Morris. This model suggests that adsorption of any material varies proportionally with \sqrt{t} , i.e., square root of time rather than with contact time t . The empirical formula used to obtain the model parameters is represented by Eq. (11)

$$q_t = k_{am} \sqrt{t} + C_{am} \quad (11)$$

where k_{am} is the rate parameter and C_{am} is the constant defining boundary layer [20].

Moreover obtained data from batch adsorption studies were fit to Boy'd film diffusion model to identify the rate-limiting step between film and intraparticle diffusion using the following Eq. (12) [7].

$$F(t) = 1 - \frac{6}{\pi^2} e^{-Bt} \quad (12)$$

$$F(t) = \frac{q_t}{q_e} \quad (13)$$

Here $F(t)$ represents the fraction adsorption capacity and B_t denotes Boy'ds number, whereas q_t and q_e stand for the MG adsorption capacity on adsorbent at given time t and at time equilibrium condition (mg/g), respectively.

Here B_t is a function of $F(t)$.

$$B_t = -0.4977 - \ln(1 - F) \quad (14)$$

From the plot of B_t vs t curves for various initial dye concentrations, it was inferred that the rate-limiting step for the adsorption process was primarily intraparticle diffusion that was driven by external mass transfer [21].

$$B_t = \frac{\pi^2 D_e}{r^2} \quad (15)$$

Effective diffusivity of dye across adsorbent particle (m^2/s) was derived by Eq. (15) where r indicates the radius of the particle and D_e is effective diffusivity radius (m^2/s).

With the assumption, such as intraparticle diffusion is negligible and isotherm is linear, the mass transfer characteristics can be best described by the following equations [7].

$$\ln \left(\frac{C_t}{C_0} - \frac{1}{mk_L + 1} \right) = \ln \left(\frac{mk_L}{1 + mk_L} \right) - \left(\frac{1 + mk_L}{mk_L} \right) k_F S_s t \quad (16)$$

$$S_s = \frac{6m}{2(1 - \epsilon_p) d_p \rho_s} \quad (17)$$

where C_0 and C_t represent the initial concentration (mg/L) of dye and at a given time (t), respectively. On the other hand, m indicates the adsorbent mass (g/L) and k_L represents the model constant for Langmuir isotherm (L/g). Similarly, k_F (cm/s) and S_s (L/cm) were represented as the mass transfer coefficient and the outer surface area of the adsorbent per unit volume, respectively.

ϵ_p represents the void space fraction of adsorbent which was estimated by the following equation [22].

$$\epsilon_p = 1 - \frac{\rho_p}{\rho_s} \quad (18)$$

where ρ_p was the apparent density (g/L) and ρ_s was the solid density of adsorbent particle (g/L).

2.11 Packed bed column experiments

A glass column of 50 cm height and 3 cm diameter was used to study the adsorption behavior of ARHC in a packed bed or fixed bed filtration column. The glass column was packed with ARHC of the required bed height. The adsorbent bed was enclosed by filter paper and glass beads of 1 cm height on the outlet end, whereas only glass beads of 1 cm height on the inlet end. The feed solution was supplied to the column using a peristaltic pump provided by Riviera. The variable experimental parameters such as; initial feed concentration (5, 10, and 20 mg/L), inlet feed flow rate (8, 12, and 16 mL/min), ARHC bed depth (2, 4, and 6 cm), and pH of feed solution (3, 6, and 9) at 303 K or 30°C. Outflow aliquots of 2-ml treated dye solutions were collected after every 10 min. The remaining dye concentration was measured using UV-spectroscopy at 617 nm wavelength. To perform the packed bed column experiments, ARHC of two different particle sizes, i.e., 150 μ m and 250 μ m, were used. However, a particle size of 150 μ m was found unsuitable due to problems like clogging, channeling, and overflowing. Therefore 250- μ m particle size was used for all column experiments.

2.12 Breakthrough curve theory

The dynamic behavior of the adsorption characteristics of the packed bed column was established using breakthrough

curves. The breakthrough curve helped us to optimize the breakthrough time (t_b) i.e. the noted time when the first colored outlet effluent was observed. Moreover the nature of the plotted C_t/C_0 vs. time, curve helped us to determine the efficiency of the packed bed column. Where C_t was the effluent concentration and C_0 was the initial inlet feed concentration. The study was performed under variable experimental parameters like initial feed, i.e., inlet dye concentration, feed flow rate, pH, and ARHC packed bed height. Observations from the set of variable parameters help us to analyze the adsorption characteristics that were estimated by the following equations.

The time equivalent to total stoichiometric capacity:

$$t_t = \int_{t=0}^{t=t_f} \left(1 - \frac{C_t}{C_0}\right) dt \tag{19}$$

Time equivalent to usable capacity:

$$tb \approx tu = \int_{t=0}^{t=t_f} \left(1 - \frac{C_t}{C_0}\right) dt \tag{20}$$

Total adsorbed mass of adsorbate:

$$S_{tot} = QC_0t_t \tag{21}$$

Adsorbed mass of adsorbate corresponding to the breakpoint:

$$S_b = QC_0t_u \tag{22}$$

Here Q was indicated as the volumetric flow rate of the inlet solution. The total mass of adsorbate injected in the column:

$$M_{tot} = QC_0t_f \tag{23}$$

where t_f is the total adsorption time required to perform the column experiment. The removal efficiency was derived as:

$$R = \frac{S_{tot}}{M_{tot}} \tag{24}$$

Equilibrium adsorbate adsorption capacity:

$$S_{eq} = \frac{S_{tot}}{m_s} \tag{25}$$

Here m_s represents the mass of adsorbent (g).

2.13 Mathematical modeling for kinetic study of packed bed continuous flow column

The ARHC packed bed column is a continuous flow column. Yoon-Nelson and Thomas model are two popular kinetic

models that were used to evaluate the adsorption behavior of MG dye on ARHC within the packed bed column. They also help to forecast the breakthrough curves which follow a general breakthrough equation of [23–25]

$$\frac{C_t}{C_0} = \frac{1}{1 + \exp^{(a-bt)}} \tag{26}$$

According to the models, the parameters can be defined as

Yoon – Nelson model : $a = k_{YN\tau}$ and $b = k_{YN}$

which on rearrangement may be written as

$$\frac{C_t}{C_0} = \frac{1}{1 + \exp^{(k_{YN}\tau - k_{YN}t)}} \tag{27}$$

Here τ is the dimensionless parameter of time for 50% of breakthrough and k_{YN} is the model constant (L/min) that was calculated using Eq. (27). Similarly,

Thomas model : $a = \frac{mk_{Th}q_0}{Q}$ and $b = k_{Th}C_0$

which on rearrangement may be written as [24, 25].

$$\frac{C_t}{C_0} = \frac{1}{1 + \exp^{\left(\frac{mk_{Th}q_0}{Q} - k_{Th}C_0t\right)}} \tag{28}$$

Here k_{Th} is the model coefficient (mL/min mg) and q_0 is ARHC fixed-bed adsorption capacity (mg/g) that was estimated using Eq. (28).

2.14 Analysis of kinetic and transport parameters of ARHC packed bed column

The flow of the effluent is unidirectional. However, on a molecular level, the effluent treatment process is composed of adsorption, advection, and dispersion. Moreover, there are biochemical and abiotic transformations that interfere with the overall removal process. These interferences can be differentiated through the following equation [26]

$$\frac{dC}{dt} = D_L \left(\frac{d^2C}{dx^2}\right) - u_0 \frac{dC}{dx} - \left(\frac{\rho_b}{\phi}\right) \frac{dS}{dt} - r_b - r_a \tag{29}$$

where C is the concentration of dye (mg/L), D_L is the longitudinal dispersion coefficient (m^2/s), and x is noted as the axial distance between the inlet and the column. On the other hand, u_0 also known as mean velocity is defined as $u_0 = Q/\phi A$ (m/s). Here ϕ stands for the porosity of the ARHC bed and A denotes the cross-sectional area of the column. For powdered amorphous charcoal used in the column has bulk density, i.e., represented as ρ_b . Biodegradation and abiotic transformation rate were denoted as r_b and r_a , respectively.

According to local equilibrium assumption, overall equilibrium adsorption can be differentiated into small hyper-local units or also known as pore scale. Thus equilibrium exists at every single adsorption point between the dissolved adsorbate and their corresponding adsorbed portion. The assumption remains valid at uniform bulk fluid flow rate and adsorbate concentration [26]. However local equilibrium assumption may not hold strong when advective equilibrium may not be established rapidly due to a rate-limiting process of diffusion. Non-equilibrium adsorption is considered to be a reversible reaction that belongs to first-order kinetics [26].

In a continuous flow column packed with ARHC, the mean pore velocity is not homogeneous due to irregular particle size. Moreover, overall pore velocity widely varies from column wall to the core of the column due to channeling and particle aggregation [27]. In such a situation, abiotic transformation and biodegradation were considered to be negligible. Thus the adsorption process may be divided into two models such as type 1 wherein adsorption corresponding to first-order equilibrium rate expression (S_1) Eq. (30,31) and type 2 wherein adsorption corresponding to non-equilibrium first-order rate expression (S_2) Eq. (32) [27].

$$S_1 = fK_d C \quad (30)$$

$$\frac{dS_1}{dt} = fK_d \frac{dC}{dt} \quad (31)$$

$$\frac{dS_2}{dt} = a[(1-f)K_d C - S_2] \quad (32)$$

Here, f and K_d are respectively represented as the fraction of active sites that correspond to type 1 adsorption phenomena and their partition coefficient (m^3/g). On the other hand, the kinetic rate constant of non-equilibrium adsorption was represented as “ a .” The total concentration of dye removal was described as $S = S_1 + S_2$.

Mass transfer behavior for two site adsorptions for linear equilibrium conditions and transfer kinetics for first-order non-equilibrium transfer may be described well by the following expression Eq. (33) [26]:

$$\frac{(1-fR_d)dC}{dt} = D_L \frac{d^2C}{dx^2} - u_0 \frac{dC}{dx} - \frac{\rho_b}{\varphi} a[(1-f)K_d C - S_2] \quad (33)$$

where retardation factor is represented by R_d and D_L was denoted as longitudinal dispersion coefficient (m^2/s) [26].

$$R_d = \frac{\rho_b K_d}{\varphi} \quad (34)$$

$$D_L = \frac{D_m}{F\varphi} + a_L u_0 \quad (35)$$

Here, D_m is presented as molecular diffusivity (m^2/s) of MG dye on ARHC, F indicates the intrinsic formation factor for fixed-bed continuous flow column, and a_L was denoted as the length of longitudinal dispersion (m). Equation 33 can be transformed into the following expression in Eq. (36) by using dimensionless variables [26].

$$(1-fR_d) \frac{dC^*}{d\tau} = \left(\frac{1}{F\varphi P_{ed}} + \frac{aL}{\langle dg \rangle} \right) \left(\frac{\langle dg \rangle}{L} \right) \left(\frac{d^2 C^*}{d\xi^2} \right) - \left(\frac{dC^*}{d\xi} \right) - \frac{D_a}{\lambda} [(1-f)K_d C_0 C^* - S_2] \quad (36)$$

$$\frac{dS_2}{d\tau} = D_a [(1-f)K_d C_0 C^* - S_2] \quad (37)$$

where is the dimensionless variables C^* and τ and ξ can be expressed as $C^* = C/C_0$, $\tau = tu_0/L$, and $\xi = x/L$. Few other dimensionless parameters were represented as:

$$P_{ed} = u_0 \frac{\langle dg \rangle}{D_m} \quad (38)$$

$$D_a = \frac{aL}{u_0} \quad (39)$$

$$\lambda = \varphi C_0 \rho_b \quad (40)$$

where P_{ed} represents Péclet number, D_a denotes the Damköhler number, and λ is dimensionless feed concentration. Equations 33–37 are only satisfied under few assumptions such as

$$\tau = 0; C^*(\xi, 0) = 0 \quad (41)$$

$$\xi = 0; C^*(\tau, 0) = 1; \frac{dS_2}{d\xi} = 0 \quad (42)$$

$$\xi = 1; \frac{dC^*}{d\xi} = 0; \frac{dS_2}{d\xi} = 0 \quad (43)$$

Equations 36 and 37 were evaluated with the continuous flow fixed bed data performed under different experimental conditions such as inlet flow rate (Q), initial concentration of dye (C_0), bed height (L_b), and pH. The equations were solved using the variable separation technique. Calculated values of parameters obtained by applying initial and boundary conditions as mentioned in Eqs. 41, 42, and 43 are presented in Table 7. Values of k_d , f , and a were estimated using software named Athena Visual Studio 14.2. The experimental

breakthrough curves were validated with numerically calculated adsorption values by a stochastic Bayesian estimator.

3 Results and discussion

3.1 Characterizations of carbon materials

The Fourier transform infrared (FTIR) characterization study of RHC and ARHC was performed using Perkin Elmer Spectrum Two. The samples were preheated at 353 K or 80 °C to remove excess moisture. Later they were mixed well with preheated potassium bromide (KBr) of 99.99% purity, provided by Merck. Adsorbent and potassium bromide mixture was pelletized at 125 kg/cm³ pressure for 3 min and tested for transmittance. Transmittance percentage (%T) vs wavenumber (cm⁻¹) graph was plotted. As represented in Figs. 1(b) and 1(d), the FTIR data centered at a common point between

1060 and 1083 cm⁻¹ due to C-O and C-C-O stretching [7, 18, 19], whereas peak at 1615 cm⁻¹ refers to C=C, characteristic C-H stretching vibration around 2916 cm⁻¹ and 3425 cm⁻¹ correspondings to the presence of OH group in the form of moisture and silica. Later peaks were not observed in the case of ARHC. This proves that ARHC is a purer form of carbon physically modified to increase total internal surface area [4].

Figures 1(a) and 1(c) represent the SEM image of RHC and ARHC at 5KX and 10KX magnification respectively, performed on Zeiss EVO MA10. Adsorbent samples were prepared by coating them with titanium before analysis using the sputter coating method. As shown in Fig. 1(a), it was observed that multiple pores were distributed in a non-homogenous manner across the RHC particle, whereas in Fig. 1(c), it was observed that pores were homogeneously layered on the surface of ARHC. It was found that due to activation of RHC into ARHC, the compact charcoal particles were broken down to

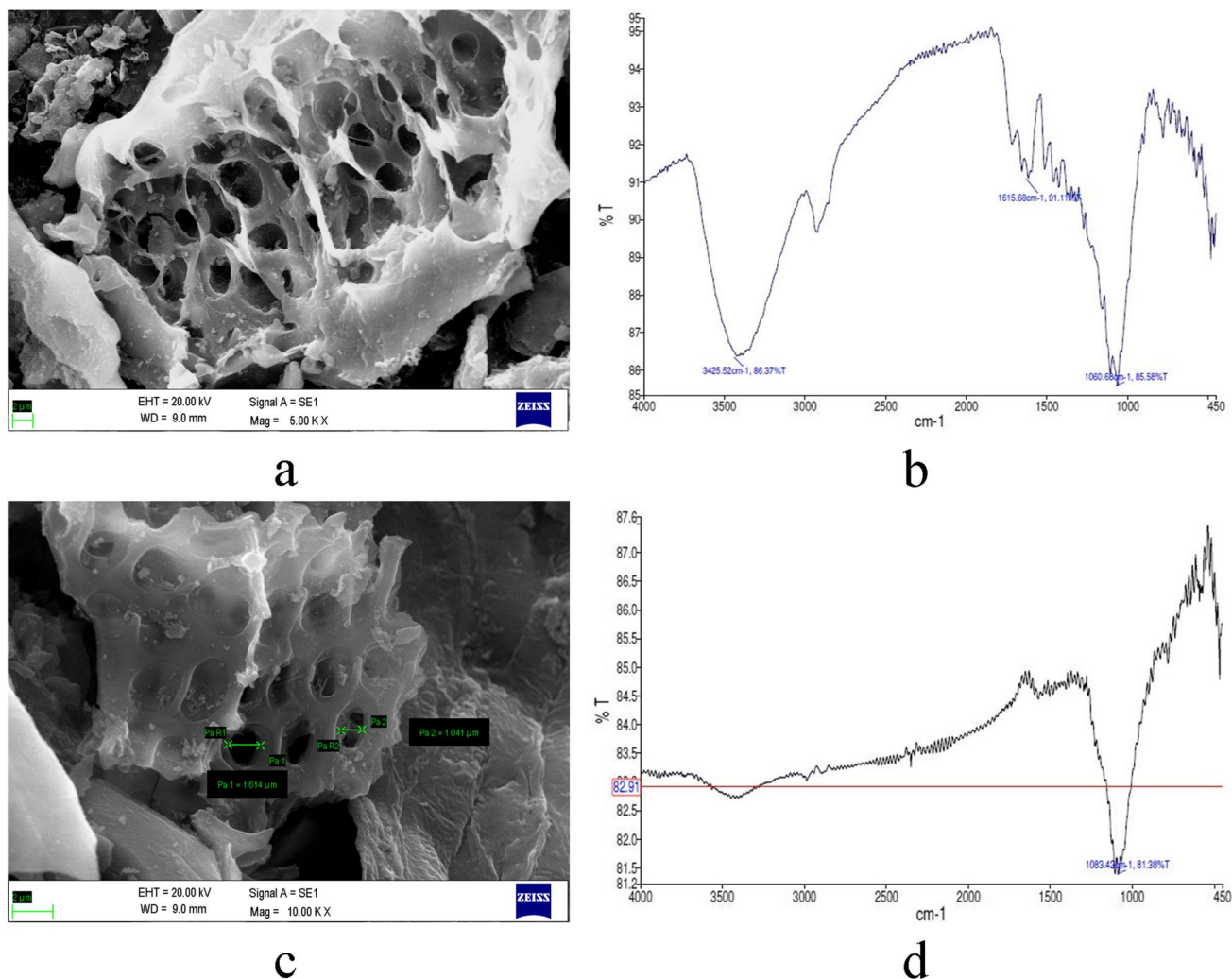
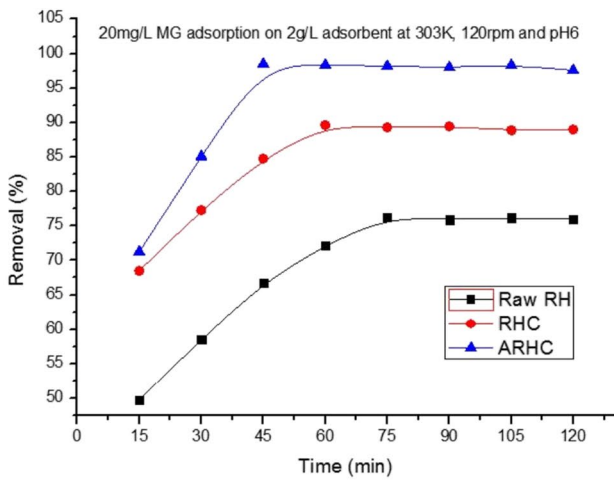
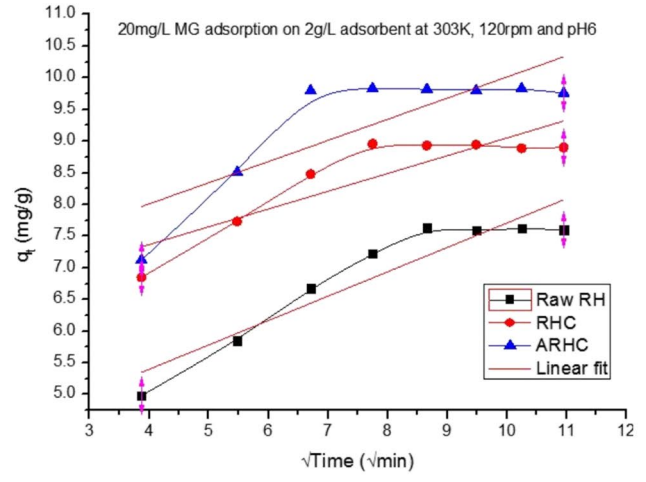


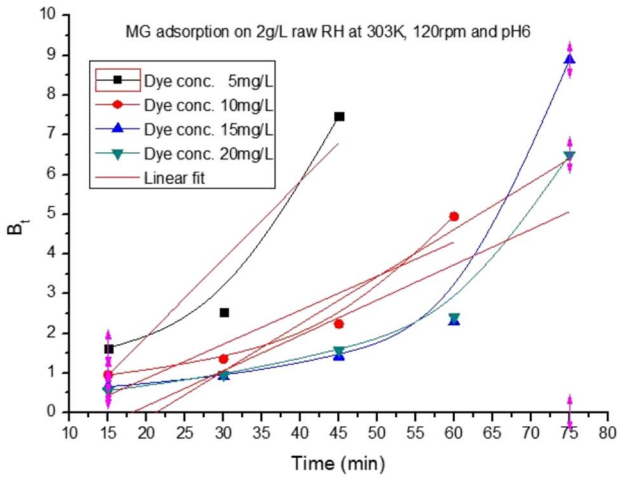
Fig. 1 (a) SEM image of RHC. (b) FTIR of RH. (c) SEM image of ARHC. (d) FTIR of ARHC



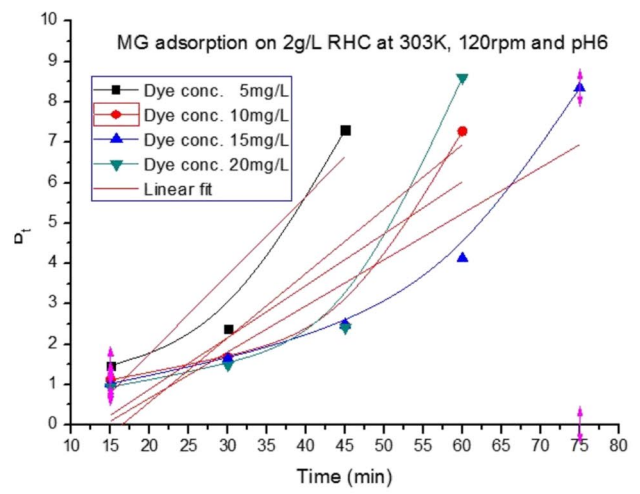
a



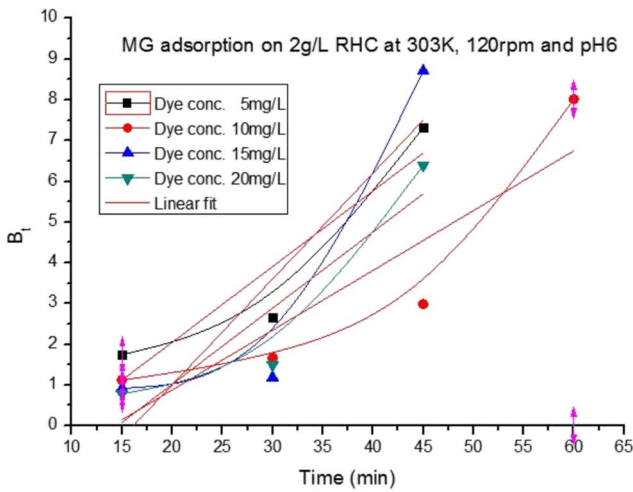
b



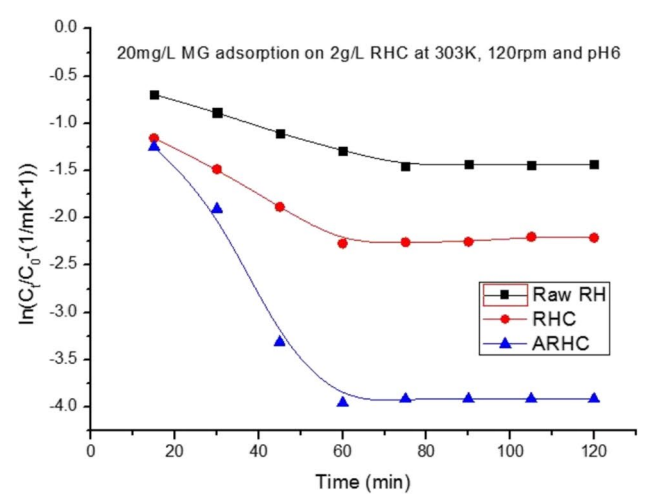
c



d



e



f

Fig. 2 (a) Effect of time on adsorption efficiency. (b) q_t vs \sqrt{t} of intra particle diffusion model. (c) B_t vs t of Boyd plot for RH. (d) B_t vs t of Boyd plot for RHC. (e) B_t vs t of Boyd plot for ARHC. f Mass transfer plot for dye adsorption on to prepared adsorbents

single-layered particles with increased numbers of pores. Such a phenomenon was suspected to occur due to the removal of silica present in rice husk.

3.2 Batch adsorption experiments

3.2.1 Effect of time

Contact period plays an important role in the adsorption process. During the contact period, the system is agitated to increase the interaction between the total adsorption surface area and the soluble dye molecules. In such a system, the batch equilibrium studies were performed at 2 g/L of adsorbent dosage to 50 ml of 20 mg/L dye solution at 7 pH and 303 K temperature for a duration until it attained equilibrium. The flasks were agitated in a shaker at 120 rpm. Samples were collected at 15 min intervals up to 120 min and concentration was analyzed. In Fig. 2(a) it was observed that with the increase in time adsorption efficiency reduces as the remaining dye concentration reduces up to a certain time, also termed as equilibrium time and then became stable. The equilibrium time for raw RH, RHC, and ARHC were found at 75 min, 60 min, and 45 min, respectively. This phenomenon was assumed to be observed as a result of the increased active adsorption site of $RH < RHC < ARHC$. Higher the adsorption surface area, faster is the rate of adsorption leading to enhanced adsorption capacity. Amongst three adsorbents, ARHC developed the maximum total internal surface area creating a shorter equilibrium time. After equilibrium time no significant adsorption takes place as sorption sites are already occupied and no further sites are available for adsorption [28]. Moreover, on prolonged agitation, the system demonstrated desorption.

3.2.2 Effect of adsorbent dosage

The time-dependent adsorption process is also driven by the amount of adsorbent used or also termed as adsorption dosage. The effect of variable dosage on adsorption efficiency was studied using a fixed feed concentration of 20 mg/L. Adsorbent dosage was varied between 2, 6, and 10 g/L at 303 K, 120 rpm, and pH 7 for 3 h. The experiment displayed an increase in removal efficiency at a higher dose of adsorbent. However, the adsorption efficiency widely varied among three adsorbents at any given dosage. It was observed that the remaining dye concentration reduced with the increase in the dosage from 2 g/L to 10 g/L. An increase in adsorbent led to the overall increase in total surface area.

A larger surface area generated a higher density of active adsorption sites. Therefore at higher adsorbent dosage, the MG dye molecules have greater access to adsorption sites leading to increased percentage removal [28, 29]. The rate of adsorption was found to decrease for higher adsorbent dosage, owing to over clouding of adsorbent leads to agglomeration. Clumping of adsorbent reduces the concentration of active site. No remarkable increase in adsorption efficiency was observed. Therefore, it was decided to work with a 2 g/L dosage for further study to avoid wastage of adsorbents.

Comparing between three adsorbents, it was noticed that ARHC displayed maximum adsorption efficiency of 98.5% dye removal. It was followed by RHC and Raw RH with 89.64% and 76.33% removal efficiency, respectively.

3.2.3 Effect of pH

The pH value of the adsorption system was found to be the most important limiting factor as the pH of the solution modifies adsorption surface characteristics. Studies were performed at various pH conditions at a constant dye concentration of 20 mg/L, 120 rpm, and 303 K. The acidic condition was not favored as adsorption capacity was found to be reduced for all three adsorbents. At acidic conditions such as pH 2, the availability of excess H^+ ions neutralizes the negatively charged active sites which were crucial for adsorption of the cationic dye [7]. It was also observed that adsorption efficiency improves at higher pH conditions such as pH 8. However, it was found that the cationic MG dye automatically decolorizes at basic pH without the adsorbent. Due to which at basic pH conditions it is difficult to distinguish between the amount of dye removed and the amount of dye decolorized. The malachite green solution has a neutral pH when dissolved in demineralized water. Therefore all further studies were performed at pH [29, 30].

3.2.4 Effect of initial dye concentration

The concentration of dye solution was varied between 5 mg/L and 20 mg/L or 5–20 ppm. The study was performed by adding 2 g/L adsorbent at 120 rpm, 303 K, and pH 6. It was observed that the removal efficiency gradually decreases at higher dye concentrations. This behavior is inverted to the adsorption behavior observed at higher adsorbent dosage. At constant dosage, increased dye concentration leads to competitive interaction between the dyes molecules to bind at the active site. ARHC displayed maximum adsorption efficiency or percentage removal of 98%, which was better than RH and RHC with 76% and 89% removal, respectively. This proves the high density of active adsorption sites available in ARHC. NaOH treatment of pyrolyzed rice husk was found to generate more mesopores by removal of SiO_2 in the form of sodium silicate. However better adsorption was

observed at lower dye concentration for all three adsorbents. On the contrary that at higher dye concentrations the active adsorption sites were occupied at a faster rate reducing the equilibrium time [28–30], the equilibrium conditions were reached within 1 h.

3.2.5 Effect of temperature

Temperature parameters were varied between 303 and 318 K or 30°C and 45°C at 20 mg/L, 120 rpm, and dosage of 2 g/L. The adsorption efficiency was studied by determining the remaining dye concentration. It was observed that adsorption efficiency reduced with an increase in temperature. Compared to other adsorbents raw, RH displayed the least adsorption efficiency with 8.3 mg/L remaining dye concentration, i.e., 58.5% removal at 318 K and maximum equilibrium time of 70 min. An increase in system temperature aggravates molecular vibrations which further reduced the availability of active sites [7]. In addition to that increasing, the temperature may also increase the rate of desorption due to high molecular mobility. In the case of raw RH, it may also lead to a swelling effect [31]. On the other hand, adsorption efficiency of RHC and ARHC was found to reduce from 90 to 71.3% and 98.5 to 80.55% with an increase in temperature from 303 to 318 K, respectively. Therefore 303 K or 30°C was considered to be the most feasible temperature for further studies.

3.2.6 Evaluation of isotherm models

The estimated values of the Langmuir isotherm model were obtained by plotting $1/q_e$ vs $1/C_e$, whereas $\log q_e$ vs $\log C_e$ plot was used to obtain Freundlich constants. The values are represented in Table 1. It was observed that Raw RH and RHC were found to fit well to both Langmuir and Freundlich isotherm models depending on the R^2 value. This phenomenon can be described as the result of the increase in MG load per unit area of adsorption surface. At lower dye load, the pollutants underwent monolayer adsorption suitable to the Langmuir isotherm model, whereas at high dye concentration and longer treatment time deposition of MG on the adsorbent surface turned multilayer, hence favoring Freundlich isotherm model [7]. On the contrary, ARHC was observed to best fit the Langmuir isotherm model. During the SEM characterization, it was observed that

homogeneously distributed pores were created on ARHC by the removal of silica from RHC. Such abundance of active adsorption sites facilitated monolayer adsorption of MG dye across the larger surface area of ARHC [7]. Therefore it was assumed that NaOH treatment of RHA extracted silica in a manner that the total internal surface area multiplied exponentially in ARHC. The maximum calculated adsorption capacity for RH, RHC, and ARHC were obtained to be 4.05, 38.46, and 1000 mg/g, respectively.

3.2.7 Adsorption kinetics for MG dye

Kinetic parameters were calculated by plotting $\log(q_e - q_t)$ vs $\text{time}(t)$ and t/q_t vs $\text{time}(t)$ for pseudo 1st and 2nd order respectively. Equilibrium adsorption capacity q_e and constant K were determined from the slope and intercept. As represented in table (2) it was observed that 2nd order fits better than 1st order for all three adsorbents with a better R^2 value. It is also reflected by the disparity between the experimental value $q_{e(\text{exp})}$ and the calculated value $q_{e1(\text{cal})}$ of 1st order model. On the other hand for 2nd order model displayed a minimum difference between the experimental and calculated value of equilibrium adsorption capacity. It was observed that the pseudo 2nd order model fits better in the case of low adsorbent concentration such as 20 mg/L i.e. used as maximum in this study Table 2.

3.2.8 Thermodynamic study

Thermodynamic parameters like spontaneity (ΔG), enthalpy (ΔH), and entropy (ΔS) were obtained from the batch adsorption experiments where adsorption behavior of three different adsorbents such as Raw RH, RHC, and ARHC was studied at four different temperature conditions. As represented in Table 3; it was observed that ΔG for Raw RH is positive at a higher temperature which makes the reaction feasible at a lower temperature. Thus poor adsorption efficiency was observed for Raw RH at a higher temperature. For RHC and ARHC, the reaction was found to be feasible as ΔG was negative. However, it was also observed that for all three adsorbent, ΔG increases with an increase in temperature. This indicates the adsorption efficiency is better at a lower temperature of 303 K. Moreover, negative ΔH suggested that the adsorption process was exothermic [32] and negative ΔS suggests that the adsorption process involves an

Table 1 Calculated parameters of Langmuir and Freundlich isotherm

Adsorbent	Temperature(°C)	Langmuir isotherm				Freundlich isotherm			
		k_L (L/mg)	Q_{max} (mg/g)	R^2	$0 < RL > 1$	k_F (mg/g)	N	R^2	
Raw RH	30	2.872093	4.05	0.997	0.0069	2.870781	1.562915	0.999	
RHC	30	0.213115	38.46	0.970	0.0857	6.637431	2.408014	0.999	
ARHC	30	0.008475	1000	0.941	0.7023	16.03245	3.027367	0.871	

Table 2 Calculated parameters of pseudofirst- and second-order kinetics

Adsorbent	Concentration	$q_{e(\text{exp})}$	Pseudo first order			Pseudo second order		
			$K_1(\text{l/min})$	$q_{e1(\text{cal})}$	R^2	K_2	$q_{e2(\text{cal})}$	R^2
RH	20 mg/L	7.63	0.055	5.53	0.656	0.011	8.47	0.997
RHC	20 mg/L	8.96	0.034	1.24	0.385	0.022	9.43	0.998
ARHC	20 mg/L	9.85	0.034	1.06	0.455	0.021	10.31	0.997

Table 3 Thermodynamic parameters of dye adsorption

Temperature(K)	Raw RH			RHC			ARHC		
	ΔG (J/mol)	ΔH (J/mol)	ΔS (J/mol K)	ΔG (J/mol)	ΔH (J/mol)	ΔS (J/mol K)	ΔG (J/mol)	ΔH (J/mol)	ΔS (J/mol K)
303	-1203	-43,848	-140.75	-3689.7	-65,797	-205.52	-8795.4	-15,4923	-485.37
308	-469.5			-2274.5			-4733.0		
313	172.24			-1371.5			-1371.5		
318	929.21			-578.49			-1924.4		

associative mechanism. Also, a negative value of ΔS reflects that no significant change occurs in the internal structures of the adsorbent during the adsorption process. Such adsorption phenomena are not favorable at high temperatures [5, 7, 32, 33].

3.2.9 Adsorption mechanism and mass transfer study for batch experiment

The adsorption mechanism of MG dye onto the adsorbents derived from rice husk was not very clear from the isotherm and the kinetic study. Thus intraparticle diffusion model based on the theory proposed by Webber and Morris (1962) was tested for all three adsorbents. According to this model $q_t \text{ vs } \sqrt{t}$ graph was plotted. The rate parameter K_{am} was calculated from the slope graphs represented in Fig. 2(b) and was found as 0.385, 0.281, and 0.331 mg/g $\sqrt{\text{min}}$ for raw RH, RHC, and ARCH, respectively. Here the intercept (C_{am}) represents the thickness of the boundary layer, i.e., greater the intercepts; thicker would be the boundary effect which was found to be 3.85842, 6.24522, and 6.6745 for raw RH, RHC, ARHC, respectively [49]. It was observed that the graphs were not linear and did not pass through the origin. Therefore it is suggested that intraparticle diffusion was not the only mechanism involved in adsorption [34]. It was assumed that interfacial surface diffusion played a vital role in association with particle diffusion [35].

Moreover, the Boyd plot of Bt vs. t at four different initial dye concentrations between 5 and 20 mg/L with 2 g/L adsorbent (Raw RH, RHC, ARHC) at 303 K and pH 6 is presented in Figs. 2 (c), 2(d), and 2(e). The obtained plots for all three adsorbents were found to be scattered. The linearized plots did not pass through the origin, which suggests

that the process of adsorption is strictly attributed to external mass transfer and the adsorption mechanism was limited to particle diffusion [36]. The values of the average effective diffusion coefficient (D_e) were found to be $5.388 \times 10^{-9} \text{ m}^2/\text{s}$, $4.324 \times 10^{-9} \text{ m}^2/\text{s}$, and $3.5404 \times 10^{-9} \text{ m}^2/\text{s}$ for Raw RH, RHC, and ARHC, respectively. Here from the values of D_e , reduced rate of diffusion was observed for RHC and ARCH compared to raw RH. It was assumed that such phenomena were observed due to the increased availability of adsorption sites on the particles of RHC and ARHC. On the contrary, raw RH has a more complex composition, owing to which external mass transfer was diffusion-dependent [36]. The values of mass transfer coefficient (K_f) were derived from the slope of $\ln\left(\frac{C_t}{C_0} - \left(\frac{1}{1+mK}\right)\right)$ vs. t curve as represented in Fig. 2(f). The computed values of K_f were 2.45×10^{-13} , 1.18×10^{-13} , and $5.09 \times 10^{-13} \text{ cm/s}$ for raw RH, RHC, and ARHC, respectively, where it was observed ARHC displayed the maximum mass transfer. The study suggested that the mass transfer of MG dye on the active adsorption site was rapid. Thus all three adsorbents were proved to be suitable for dye adsorption with ARHC as the best performing adsorbent.

3.3 Fixed bed continuous flow column experiments

3.3.1 Effect of pH on column adsorption behavior

Previously during the parameter study of pH in a batch adsorption system, it was mentioned that pH 6 was considered as the most suitable condition to avoid ambiguity between the rate of adsorption and mere decolorization. During the batch adsorption study, it was observed that MG decolorizes at the basic pH range which was reversible by

readjusting the solution to neutral pH. On the other hand, the decolorized basic dye solution was subjected to adsorption on all of the three adsorbents. Then the treated solutions were readjusted to neutral pH. It was observed that for a given combination of parameters, the removal efficiency remained similar to the non-adjusted solution with negligible deviation. However, the effect of pH on adsorption of MG on ARHA packed bed column was studied between 3, 7, and 9 with inlet feed flow rate of 8 ml/min, bed height of 2 cm, and initial dye concentration of 50 mg/L.

It was observed from Fig. 3(a) that breakthrough time gradually increased with an increase in the pH of the system. The breakthrough time was noted to be 30, 150, and

190 min for pH 3, 6, and 9, respectively. In acidic solution, MG adsorption on ARHC is suspected to reduce because of high H⁺ ion concentration. On the other hand, better adsorption efficiency was observed at higher pH due to the deprotonation of the active sites [33].

3.3.2 Effect of ARHC bed height on column adsorption behavior

In a fixed bed adsorption system, height of the adsorbent column plays a crucial role in the evaluation of adsorption efficiency. The height of the column facilitates intrinsic interaction between adsorbent and dye molecule. The study

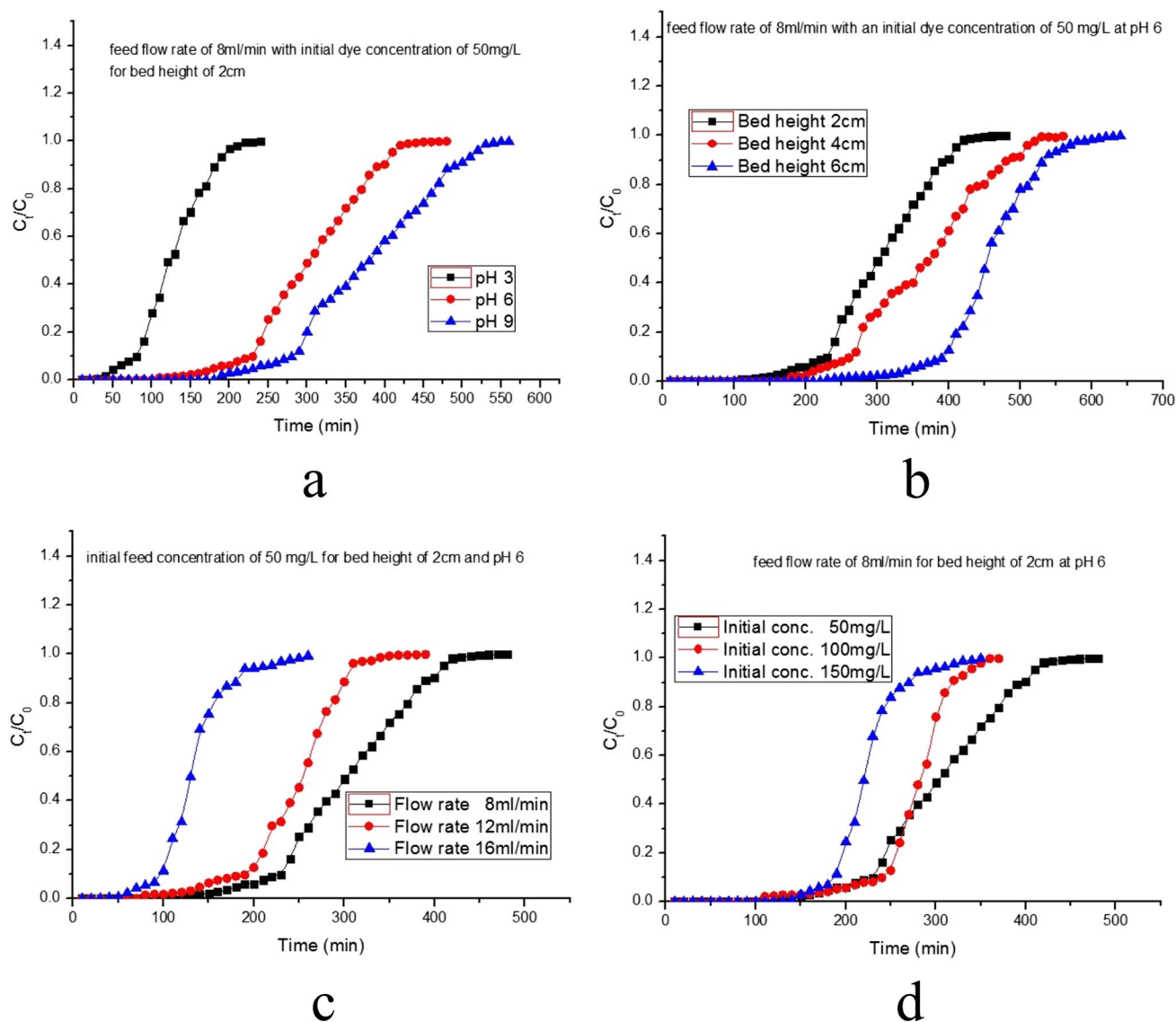


Fig. 3 (a) Effect of pH on breakthrough curve. (b) Effect of bed height on breakthrough curve. (c) Effect of flow rate on breakthrough curve. (d) Effect of dye concentration on breakthrough curve

was conducted at different bed heights of 2, 4, and 6 cm at a feed flow rate of 8 ml/min with an initial dye concentration of 50 mg/L at pH 7.

As presented in Fig. 3(b), a longer breakthrough time was observed at a higher bed height. The breakthrough time observed was at 150, 185, and 230 min for 2, 4, and 6 cm bed height, respectively. An increase in bed height directly leads to an increase in adsorbent dosage. The increased amount of adsorbent expanded the total surface area of the adsorbent that generated more active sites for adsorption. Thus it was observed that at higher bed height, the interaction between MG dye molecule and active sites increased leading to better adsorption capacity [33].

3.3.3 Effect of inlet flow rate on column adsorption behavior

Inlet feed flow rate influences the breakthrough parameters exponentially. The impact of flow rate on adsorption behavior of the continuous flow fixed-bed column was studied by varying the inlet flow rate between 8, 12, and 16 mL/min at an initial feed concentration of 50 mg/L for bed height of 2 cm and pH 7.

From the curves plotted by C_t/C_0 vs time (Fig. 3(c)), it was observed that time required to attain breakthrough considerably reduced from 150 to 75 min with an increase in inlet feed flow rate from 8 ml/min to 16 ml/m. It was from the parameters obtained from the fixed bed column study interpreted that an apparent decrease in adsorption capacity due to an increase in flow rate was attributed to increased availability of dye molecules per active site. It was also suggested that a reduction in breakthrough time is observed due to an increased rate of active site saturation. This phenomenon also supports the assumption of enhanced mass transfer rate with an increase in inlet feed flow rate, thereby increasing dye adsorption [7, 33].

3.3.4 Effect of inlet dye concentration on column adsorption behavior

The study was conducted by varying initial feed concentration of dye solution between 50 mg/L, 100 mg/L, and 150 mg/L for a fixed bed of 2 cm height, with a feed flow rate of 8 mL/min.

In Fig. 3(d) it was observed that breakthrough time was attained faster at a higher concentration of feed solution [37]. A similar phenomenon was observed at a higher feed flow rate. The breakthrough time was noted to be 95, 115, and 150 min for 50, 100, and 150 mg/L dye concentration, respectively. Thus it was assumed that a lower feed concentration rate of saturation is much lower than compared to high feed concentration or feed flow rate. From Fig. 3(d) it was also observed that the slope was steeper at higher feed concentration indicating a higher rate of adsorption, thereby shortening the breakthrough time [7]. Breakthrough parameters were evaluated as represented in Table 4.

3.3.5 Kinetic modeling for MG adsorption on fixed bed continuous flow column

Yoon-Nelson model represented in Eq. (27) was evaluated by experimental data obtained from adsorption of MG dye on fixed bed continuous flow column at various column conditions. The theoretical breakthrough curves were predicted by solving the Avramiequation (44) using Microsoft Excel solver[38, 39]. The term k_{YN} symbolizes adsorption rate constant dependent on dimensionless time τ . The calculated values of k_{YN} (L/min) and τ are represented in Table 4, where it was noticed that for the column conditions of bed height 6 cm, pH 6 and 8 ml/min the obtained k_{YN} was noted to be equal to $K_2=0.021$, i.e., pseudo 2nd order adsorption rate constant for ARHC. Therefore it was assumed that k_{YN} and K_2 are time-dependent and independent of MG

Table 4 Calculated values of model parameters for MG removal on ARHC column

Bed height (cm)	Experimental conditions			Yoon-Nelson model			Thomas model		
	pH	Concentration (mg/L)	Flow rate (ml/min)	K_{YN} (L/min)	τ (min)	R^2	q_0 (mg/g)	K_{TH} ($\times 10^{-3}$ L/mg min)	R^2
6	6	50	8	0.021	461.6	0.977	1.26	0.44	0.977
4	6	50	8	0.022	368.864	0.962	1.281	0.5	0.962
2	6	50	8	0.03	311.5	0.966	3.738	0.6	0.966
2	6	50	16	0.045	149.044	0.959	8.048	0.9	0.959
2	6	50	12	0.035	232.343	0.967	5.69	0.7	0.967
2	6	150	8	0.048	194.25	0.973	1.989	0.32	0.973
2	6	100	8	0.036	267	0.874	2.307	0.36	0.874
2	9	50	8	0.022	384.454	0.946	2.48	0.44	0.946
2	3	50	8	0.047	127.468	0.985	3.75	0.94	0.985

concentration in the adsorption system. From Fig. 4 it was also observed that the calculated breakthrough graph was following the experimental C_t/C_0 vs τ graph [33].

$$\frac{C_t}{C_0} = \frac{A}{1 + \exp(k_{YN}\tau - k_{YN}t)} \tag{44}$$

where A was denoted as Avrami constant and T was the temperature in kelvin and t was time.

Thomas model was estimated using experimental data obtained from fixed-bed continuous flow column as represented by Eq. 28. Calculated values of Thomas kinetic parameters such as kinetic coefficient (k_{Th}), dye adsorption capacity (q_0), and regression coefficient (R^2) at given experimental conditions are shown in Table 4. The values of k_{Th} and q_0 give us a clear idea about the adsorption rate constant and adsorption capacity of ARHC at various column conditions.

It was inferred that the experimentally obtained data from fixed-bed continuous flow column adsorption fits both Yoon-Nelson and Thomas models well as correlation coefficients range between $0.9 < R^2 < 0.985$.

3.3.6 Estimation of transport and kinetic parameters for MG dye on ARHC column

Parameter values of the fixed bed continuous flow adsorption experimental system are presented in Table 5. Adsorption parameters were estimated as functions of dimensionless numbers (τ) (Eq. 28–42) are presented in Table 6. It was observed that for a given combination of fixed parameters including small bed height and low flow rate had reduced the chance of pore velocity fluctuations. It was observed that the distribution of dye feed solution was more stable and uniform across the fixed bed column at low flow rates. This facilitates better interaction between the adsorbent and dissolved dye molecules. A low flow rate was also found to established adsorption equilibrium over the maximum volumetric surface of the ARHC column at a cost of higher breakthrough time. The breakthrough curve at a low flow rate imitated the 1-site adsorption equilibrium model (Table 6) satisfactorily. On the other hand, at a higher flow rate and bed height adsorption mechanism was observed to colonize at separate non-interacting sites. This was assumed to cause due to fluctuation of pore velocity leading to the establishment of non-equilibrium and channeling of a column. Thus at a higher flow rate, the adsorption system fits the 2-site model better. The Damköhler number (D_a), is defined as the ratio between times taken for convective flow and adsorption time. Convective flow refers to the flow behavior of the feed across a laminar cross-section of the column. In short slower the convective flow, the longer will the interaction time between dye and adsorbent. Thus in an ideal situation, the convective flow should be slower than the rate of adsorption. This study revealed that convective flow was faster than the rate of adsorption at higher flow rates. The kinetic parameter, ‘a’ depends on the adsorption kinetics and diffusive transfer of the dye molecule. The adsorption mechanism was revealed to be a combined effect of surface diffusion and intraparticle diffusion. Dissolved dye molecules from the bulk solution travel towards the

Table 5 Experimental values of kinetic parameter

Parameters	Value
D (cm)	3 cm
L	50 cm
Φ	0.45
ρ_b	317.4×10^3 mg/L
D_m	3.5404×10^{-5} cm ² /sec
L_b	2 cm, 4 cm, 6 cm
dg	0.005 cm
a_L	0.005 cm
C_0	50 mg/L, 100 mg/L, 150 mg/L

Table 6 Evaluated parameters as functions of dimensionless numbers for ARHC column

$u_0 = Q/fi$ A (cm/min)	L_b/D	P_{ed}	$\lambda = \Phi C_0/\rho_b$	f	k_d (m ³ /kg)	a (1/min)	$k_d^* = k_d \times C_0$ (g/g)	$D_a = aL/u_0$
2.516316741	0.6667	5.922863569	7.08885E-05	0.903	1.293	0.0056	0.06465	0.11127375
2.516316741	1.3333	5.922863569	7.08885E-05	0.594	0.5724	0.0004	0.02862	0.007948125
2.516316741	2.00	5.922863569	7.08885E-05	0.504	0.8907	0.0004	0.04453	0.007948125
3.774475112	0.6667	8.884295353	7.08885E-05	0.57	3.5442	0.0008	0.17721	0.0105975
5.032633483	0.6667	11.84572714	7.08885E-05	0.51	1.8486	0.001	0.09243	0.009935156
2.516316741	0.6667	5.922863569	0.000141777	0.742	0.2166	0.0125	0.02166	0.248378906
2.516316741	0.6667	5.922863569	0.000212665	0.603	0.2259	0.0045	0.03388	0.089416406
2.516316741	0.6667	5.922863569	7.08885E-05	0.541	0.1664	0.0065	0.00832	0.129157031
2.516316741	0.6667	5.922863569	7.08885E-05	0.793	0.304	0.0095	0.0152	0.188767969

adsorbent surface via diffusive transport. This leads to the formation of a boundary layer around the adsorbent’s outer surface [7]. Results revealed that values of “a” increased with a reduction in boundary layer thickness. Dimensionless partition coefficient, $K_d^* = K_d \times C_0$ also represents the adsorption capacity of ARHC bed at saturated condition. Active pore sites were distributed heterogeneously due to an increase in ARHC column height, feed flow rate, and initial dye concentration. This leads to fluctuation in pore velocity and reduction in fractional equilibrium sites and therefore reduces the overall adsorption efficiency[26]. The adsorption capacity of the fixed bed column K_d^* was found to increase with the increase in dye feed concentration due

to rapid adsorption and early attainment of saturation conditions. It was also observed that experimental breakthrough curves were in agreement with the breakthrough curves that were predicted numerically as represented in Fig. 4.

4 Comparison with other adsorbents

While comparing with other adsorbents for MG removal it was found that the present study takes place at a shorter treatment period and room temperature (Table 7).From the comparative study it was also observed that all the adsorbents used by researchers were not widely available with lower adsorption capacity compared to the adsorbents

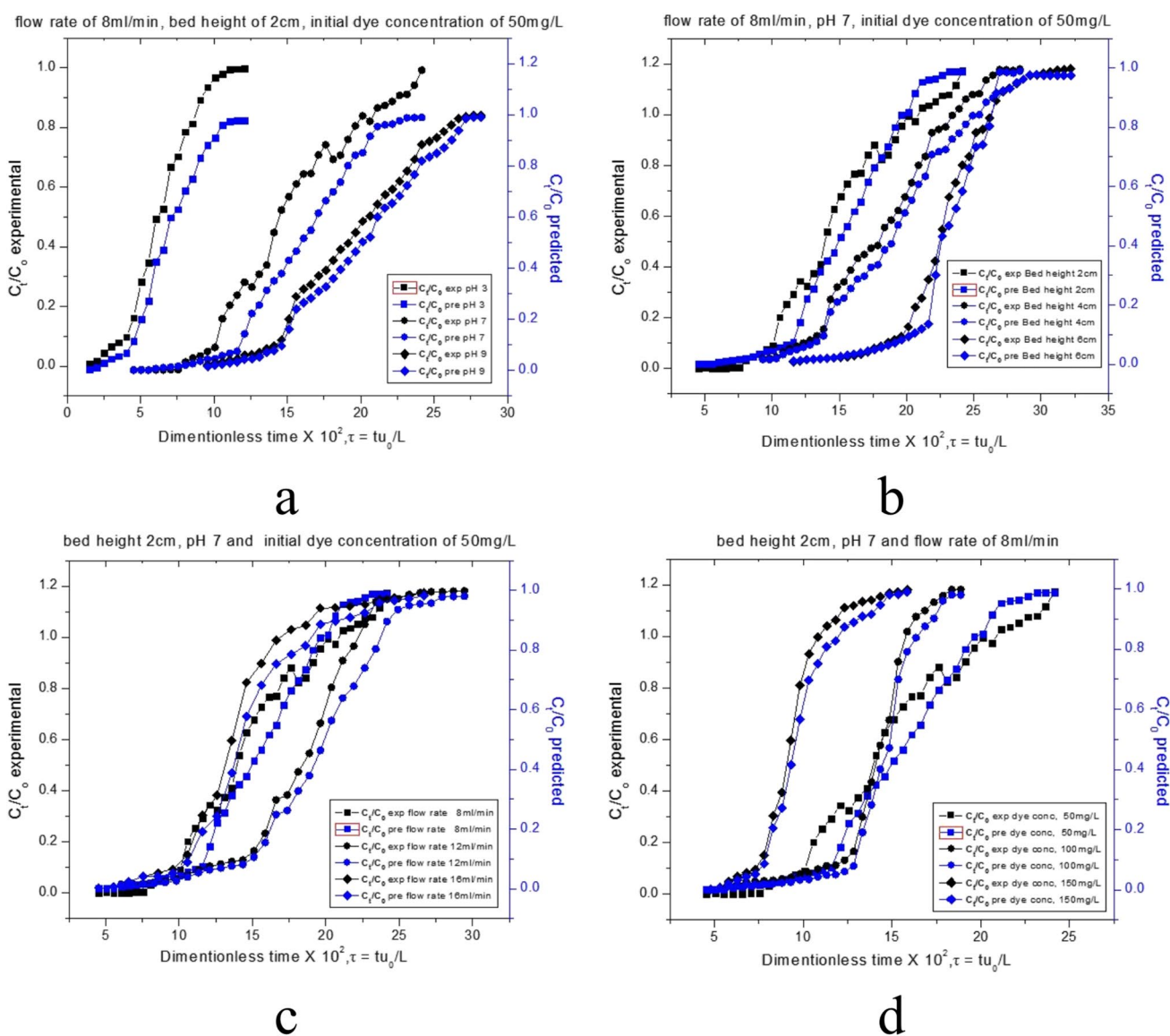


Fig. 4 Comparative representation between experimentally measured and numerically predicted breakthrough curves with respect to (a) pH of the dye solution, (b) column bed height, (c) feed flow rate, and (d) dye concentration

Table 7 Comparison of MG adsorption capacity on RH, RHC, and ARHC with other adsorbents

Adsorbent	Adsorption capacity (mg/g)	Condition		References
		pH	Temp. (K)	
Carbonised <i>Borassus</i> bark	20.70	6	303	[40]
Dry potato peel	32.39	4	298	[41]
Dried <i>Solanum tuberosum</i> leaf	33.3	7	303	[42]
Sawdust of Neem tree	4.35	7.2	303	[43]
Wood Sawdust of Rubber tree	36.45	–	305	[44]
Commercial activated carbon	8.27	7	303	[45]
Cellulose powder	2.422	7.2	298	[46]
Raw rice husk	4.05	6	303	Present study
Rice husk charcoal	38.46	6	303	Present study
Activated rice husk charcoal	1000	6	303	Present study

used in the current study. The overall cost for production of ARHC was found to be Rs. 150.00/Kg. On this basis, it could be concluded that RH, RHC, and ARHC are economical, efficient, and effective adsorbents as compared to other adsorbents.

5 Conclusion

The present work showed that raw rice husk and activated carbon derived from rice husk charcoal were reliable and promising adsorbents for the removal of Malachite Green dye over a wide range of concentrations. Between the three adsorbents, ARHC was found to be the best performing adsorbent. Data obtained from the adsorption system at equilibrium condition were fitted to isotherm models such as Langmuir and Freundlich model. From the batch adsorption experiments it was found that unlike raw RH and RHC equilibrium data for ARHC fitted best to Langmuir model. The adsorption kinetics for all three adsorbents were observed to fit the Pseudo second-order model better indicating that the overall rate of the adsorption process was controlled by both physisorption and chemisorptions that involve valency exchange between the sorbent and sorbate. The adsorption mechanism was mainly found to be surface diffusion along with intraparticle diffusion that was governed by external mass transfer. The negative value of ΔH obtained from the thermodynamic study indicates that the process is exothermic. Moreover, fixed-bed column studies were performed using ARHC as the adsorbent. At different experimental conditions such as inlet flow rate (Q), initial dye concentration (C_0), bed height (L_b), and pH, it was observed that the adsorption capacity (k_d^*) of MG dye on ARHC in a fixed bed continuous flow in a column mode, ranged between 0.008 and 0.177 (g/g). The experimental breakthrough curve was in proximity to the predicted curve which proves that ARHC possesses a

high adsorption capacity towards dissolved malachite green (MG) in wastewater. It was concluded that RH, RHC, and ARHC can be used as efficient and environment-friendly adsorbents for the removal of dissolved malachite green from contaminated water. However, ARHC was proved to be the best-suited candidate among the three adsorbents. During this present study, it was concluded that activated rice husk (ARHC) can be a packed in any adsorption column or cartridge that was suitable to treat dye-contaminated water in both domestic and industrial scale. Moreover the secondary product such as sodium silicate and precipitated bio silica obtained from rice husk charcoal are of great economic value.

Acknowledgements The authors wish to thank the Dalmia Holding Groups for the financial support and also thankful to the Dept. of Chemical Engineering, Jadavpur University, for their great facilities and support.

Authors' contributions NS had done all the experimental work and preparing the manuscript; LD also prepared the manuscript; and PD, AB, and CB supervised the work.

Funding The authors wish to thank the Dalmia Holding Groups for the financial support.

Data availability Data will be provided on request.

Declarations

Conflict of interest The authors declare no competing interests.

7. References

1. Rajan MR DNS (2014) Impact of Dyeing Industry Effluent on Groundwater Quality by Water Quality Index and Correlation Analysis. J Pollut Eff Control 02: <https://doi.org/10.4172/2375-4397.1000126>

2. Culp SJ, Mellick PW, Trotter RW, et al (2006) Carcinogenicity of malachite green chloride and leucomalachite green in B6C3F1 mice and F344 rats. *Food Chem Toxicol* 44: <https://doi.org/10.1016/j.fct.2006.01.016>
3. Nigam P, Banat IM, Singh D, Marchant R (1996) Microbial process for the decolorization of textile effluent containing azo, diazo and reactive dyes. *Process Biochem* 31: [https://doi.org/10.1016/0032-9592\(95\)00085-2](https://doi.org/10.1016/0032-9592(95)00085-2)
4. Ganguly P, Sarkhel R, Das P (2020) Synthesis of pyrolyzed biochar and its application for dye removal: Batch, kinetic and isotherm with linear and non-linear mathematical analysis. *Surfaces and Interfaces* 20: <https://doi.org/10.1016/j.surfin.2020.100616>
5. Chakraborty V, Das P, Roy PK (2021) Graphene oxide-coated pyrolysed biochar from waste sawdust and its application for treatment of cadmium-containing solution: batch, fixed-bed column, regeneration, and mathematical modelling. *Biomass Convers Biorefinery*. <https://doi.org/10.1007/s13399-020-01153-7>
6. Dushenkov V, Kumar PBAN, Motto H, Raskin I (1995) Rhizofiltration: The Use of Plants to Remove Heavy Metals from Aqueous Streams. *Environ Sci Technol* 29: <https://doi.org/10.1021/es00005a015>
7. Das L, Sengupta S, Das P, et al (2021) Experimental and Numerical modeling on dye adsorption using pyrolyzed mesoporous biochar in Batch and fixed-bed column reactor: Isotherm, Thermodynamics, Mass transfer, Kinetic analysis. *Surfaces and Interfaces* 23: <https://doi.org/10.1016/j.surfin.2021.100985>
8. Periasamy K, Namasiyayam C (1996) Removal of copper(II) by adsorption onto peanut hull carbon from water and copper plating industry wastewater. *Chemosphere* 32: [https://doi.org/10.1016/0045-6535\(95\)00332-0](https://doi.org/10.1016/0045-6535(95)00332-0)
9. Kalavathy MH, Karthikeyan T, Rajgopal S, Miranda LR (2005) Kinetic and isotherm studies of Cu(II) adsorption onto H3PO4-activated rubber wood sawdust. *J Colloid Interface Sci* 292: <https://doi.org/10.1016/j.jcis.2005.05.087>
10. Badmus M, Audu T, Anyata B (2007) Removal of lead ion from industrial wastewaters by activated carbon prepared from periwinkle shells (*Typanotonus fuscatus*). *Turkish J Eng Environ Sci* 31:251–263
11. Madhavarao M, Ramesh A, Purnachandrarao G, Seshaiiah K (2006) Removal of copper and cadmium from the aqueous solutions by activated carbon derived from Ceiba pentandra hulls. *J Hazard Mater* 129: <https://doi.org/10.1016/j.jhazmat.2005.08.018>
12. Namasiyayam C, Kadirvelu K (1997) Agricultural solid wastes for the removal of heavy metals: Adsorption of Cu(II) by coirpith carbon. *Chemosphere* 34: [https://doi.org/10.1016/S0045-6535\(96\)00384-0](https://doi.org/10.1016/S0045-6535(96)00384-0)
13. Gidde MRJAP, Jivan AP (2007) Waste to Wealth. Potential of Rice Husk in India a Literature Review. In: *International Conference on Cleaner Technologies and Environmental Management PEC*. Pondicherry, pp 586–590
14. Zain MFM, Islam MN, Mahmud F, Jamil M (2011) Production of rice husk ash for use in concrete as a supplementary cementitious material. *Constr Build Mater* 25: <https://doi.org/10.1016/j.conbuildmat.2010.07.003>
15. Imagawa A, Seto R, Nagaosa Y (2000) Adsorption of chlorinated hydrocarbons from air and aqueous solutions by carbonized rice husk. *Carbon N Y* 38: [https://doi.org/10.1016/S0008-6223\(00\)00006-3](https://doi.org/10.1016/S0008-6223(00)00006-3)
16. Singh B (2018) Rice husk ash. In: *Waste and supplementary cementitious materials in concrete: Characterisation, Properties and Applications*. Elsevier, pp 417–460
17. Todkar BS, Deorukhkar OA, Deshmukh SM (2016) Extraction of Silica from Rice Husk. *Int J Eng Res Dev* 12:69–74
18. Khan EA, Shahjahan, Khan TA (2018) Adsorption of methyl red on activated carbon derived from custard apple (*Annona squamosa*) fruit shell: Equilibrium isotherm and kinetic studies. *J Mol Liq* 249: <https://doi.org/10.1016/j.molliq.2017.11.125>
19. Das L, Das P, Bhowal A, Bhattacharjee C (2020) Synthesis of hybrid hydrogel nano-polymer composite using Graphene oxide, Chitosan and PVA and its application in waste water treatment. *Environ Technol Innov* 18: <https://doi.org/10.1016/j.eti.2020.100664>
20. Banerjee P, Das P, Zaman A, Das P (2016) Application of graphene oxide nanoplatelets for adsorption of Ibuprofen from aqueous solutions: Evaluation of process kinetics and thermodynamics. *Process Saf Environ Prot* 101: <https://doi.org/10.1016/j.psep.2016.01.021>
21. Boyd GE, Adamson AW, Myers LS (1947) The exchange adsorption of ions from aqueous solutions by organic zeolites. II. Kinetics¹. *J Am Chem Soc* 69: <https://doi.org/10.1021/ja01203a066>
22. Dotto GL, Buriol C, Pinto LAA (2014) Diffusional mass transfer model for the adsorption of food dyes on chitosan films. *Chem Eng Res Des* 92: <https://doi.org/10.1016/j.cherd.2014.03.013>
23. Song W, Xu X, Tan X, et al (2015) Column adsorption of perchlorate by amine-crosslinked biopolymer based resin and its biological, chemical regeneration properties. *Carbohydr Polym* 115: <https://doi.org/10.1016/j.carbpol.2014.09.010>
24. Tan KL, Hameed BH (2017) Insight into the adsorption kinetics models for the removal of contaminants from aqueous solutions. *J Taiwan Inst Chem Eng* 74: <https://doi.org/10.1016/j.jtice.2017.01.024>
25. Dima JB, Ferrari M, Zaritzky N (2020) Mathematical modeling of fixed-bed columns adsorption: hexavalent chromium onto chitosan flakes. *Ind Eng Chem Res* 59: <https://doi.org/10.1021/acs.iecr.0c02004>
26. Magga Z, Tzovolou DN, Theodoropoulou MA, et al (2008) Soil column experiments used as a means to assess transport, sorption, and biodegradation of pesticides in groundwater. *J Environ Sci Heal Part B* 43: <https://doi.org/10.1080/03601230802388868>
27. Harmon TC, Ball WP, Roberts PV (2015) Nonequilibrium transport of organic contaminants in groundwater
28. Ali F, Bibi S, Ali N, et al (2020) Sorptive removal of malachite green dye by activated charcoal: Process optimization, kinetic, and thermodynamic evaluation. *Case Stud Chem Environ Eng* 2: <https://doi.org/10.1016/j.cscee.2020.100025>
29. Sartape AS, Mandhare AM, Jadhav V V., et al (2017) Removal of malachite green dye from aqueous solution with adsorption technique using *Limonia acidissima* (wood apple) shell as low cost adsorbent. *Arab J Chem* 10: <https://doi.org/10.1016/j.arabjce.2013.12.019>
30. Garg V., Kumar R, Gupta R (2004) Removal of malachite green dye from aqueous solution by adsorption using agro-industry waste: a case study of *Prosopis cineraria*. *Dye Pigment* 62: <https://doi.org/10.1016/j.dyepig.2003.10.016>
31. Bao Y, Zhang G (2012) Study of adsorption characteristics of methylene blue onto activated carbon made by *Salix Psammophila*. *Energy Procedia* 16: <https://doi.org/10.1016/j.egypro.2012.01.182>
32. Chowdhury S, Saha P (2010) Sea shell powder as a new adsorbent to remove Basic Green 4 (Malachite Green) from aqueous solutions: Equilibrium, kinetic and thermodynamic studies. *Chem Eng J* 164: <https://doi.org/10.1016/j.cej.2010.08.050>
33. Chowdhury S, Chakraborty S, Saha P Das (2013) Response surface optimization of a dynamic dye adsorption process: a case study of crystal violet adsorption onto NaOH-modified rice husk. *Environ Sci Pollut Res* 20: <https://doi.org/10.1007/s11356-012-0989-7>
34. Mohanty K, Naidu JT, Meikap BC, Biswas MN (2006) Removal of Crystal Violet from Wastewater by Activated Carbons Prepared from Rice Husk. *Ind Eng Chem Res* 45: <https://doi.org/10.1021/ie060257r>

35. Sarkar M, Santra D (2015) Modeling fluoride adsorption on cerium-loaded cellulose bead—response surface methodology, equilibrium, and kinetic studies. *Water, Air, Soil Pollut* 226:. <https://doi.org/10.1007/s11270-015-2307-8>
36. Tan IAW, Hameed BH (2010) Adsorption isotherms, kinetics, thermodynamics and desorption studies of basic dye on activated carbon derived from oil palm empty fruit bunch. *J Appl Sci* 10:. <https://doi.org/10.3923/jas.2010.2565.2571>
37. Ahmad AA, Hameed BH (2010) Fixed-bed adsorption of reactive azo dye onto granular activated carbon prepared from waste. *J Hazard Mater* 175:. <https://doi.org/10.1016/j.jhazmat.2009.10.003>
38. Sha W, Wu X, Keong KG (2011) Modelling the thermodynamics and kinetics of crystallisation of nickel–phosphorus (Ni–P) deposits. In: *Electroless Copper and Nickel–Phosphorus Plating*. Elsevier
39. Yagub MT, Sen TK, Afroze S, Ang HM (2015) Fixed-bed dynamic column adsorption study of methylene blue (MB) onto pine cone. *Desalin Water Treat* 55:. <https://doi.org/10.1080/19443994.2014.924034>
40. Hema M, Martin P, Prasath D, Arivoli S (2009) Adsorption of malachite green onto carbon prepared from borassus bark. *Arab J Sci Eng* 34:
41. Guechi E-K, Hamdaoui O (2016) Sorption of malachite green from aqueous solution by potato peel: Kinetics and equilibrium modeling using non-linear analysis method. *Arab J Chem* 9:. <https://doi.org/10.1016/j.arabjc.2011.05.011>
42. Gupta N, Kushwaha AK, Chattopadhyaya MC (2016) Application of potato (*Solanum tuberosum*) plant wastes for the removal of methylene blue and malachite green dye from aqueous solution. *Arab J Chem* 9:. <https://doi.org/10.1016/j.arabjc.2011.07.021>
43. Khattri SD, Singh MK (2009) Removal of malachite green from dye wastewater using neem sawdust by adsorption. *J Hazard Mater* 167:. <https://doi.org/10.1016/j.jhazmat.2009.01.101>
44. Vasanth Kumar K, Sivanesan S (2007) Isotherms for Malachite Green onto rubber wood (*Hevea brasiliensis*) sawdust: Comparison of linear and non-linear methods. *Dye Pigment* 72:. <https://doi.org/10.1016/j.dyepig.2005.07.021>
45. Mall ID, Srivastava VC, Agarwal NK, Mishra IM (2005) Adsorptive removal of malachite green dye from aqueous solution by bagasse fly ash and activated carbon-kinetic study and equilibrium isotherm analyses. *Colloids Surfaces A Physicochem Eng Asp* 264:. <https://doi.org/10.1016/j.colsurfa.2005.03.027>
46. Pradeep Sekhar C, Kalidhasan S, Rajesh V, Rajesh N (2009) Biopolymer adsorbent for the removal of malachite green from aqueous solution. *Chemosphere* 77. <https://doi.org/10.1016/j.chemosphere.2009.07.068>

Publisher's note Springer Nature remains neutral with regard to jurisdictional claims in published maps and institutional affiliations.